Electronic Supplementary Material (ESI) for Journal of Materials Chemistry C.
This journal is © The Royal Society of Chemistry 2023

Electronic Supplementary Information

A Photo-Responsive Organic Electrochemical Transistor

Nicholas Turetta, [a] Wojciech Danowski, [a] Luca Cusin, [a] Pietro Antonio Livio, [a] Rawad Hallani, [b] Iain McCulloch [bc] and Paolo Samorì *[a]

Affiliations

a. University of Strasbourg, CNRS, ISIS UMR 7006, 8 allée Gaspard Monge, F-67000 Strasbourg, France.
b. University of Oxford, Department of Chemistry, Oxford, OX1 3TA, UK.
c. King Abdullah University of Science and Technology (KAUST), KAUST Solar Center (KSC), Thuwal, 23955-6900, Saudi Arabia.

Table of contents:

1 Synthesis of Materials

General Considerations

All reagents from commercial sources such as Aldrich, TCI, Fluorochem, BDLPharm were used as received. Anhydrous solvents were obtained from commercial sources and used without any further purification (Aldrich, Acros). Column chromatography was performed using silica gel (SiO_2) from VWR (40-63 µm) NMR spectra were recorded on Bruker Ascend Avance Neo – 500 MHz (^{1}H: 500 MHz, ^{13}C: 125 MHz) spectrometer. Chemical shifts are reported in parts per million (ppm) relative to the residual solvent signal (for $CDCl_3$ δ 7.26 for 1H, δ 77.16 for ^{13}C). For ^{1}H NMR spectroscopy, the splitting pattern of peaks is designated as follows: s (singlet), d (doublet), t (triplet), m (multiplet), br (broad), or dd (doublet of doublets). High resolution mass spectrometry (HRMS) was performed on a LTQ Orbitrap XL spectrometer with electrospray ionization (ESI). The NMR spectra of spiropyrans were recorded in $CDCl_3$ filtrated over a short plug of K_2CO_3.

Procedures

Poly(2-(4,4′-bis(2-methoxyethoxy)-5′-methyl-[2,2′-bithiophen]-5-yl)-5-methylthieno [3,2-b]thiophene) (**pgBTTT**) polymer has been synthesized as previously reported in the literature.[1]

The two precursors, 5,5'-dibromo-4,4'-bis(2-(2-(2-methoxyethoxy)ethoxy)ethoxy)-2,2'-bithiophene (100 mg, 0.15 mmol, 1 eq.) and 2,5-bis(trimethylstannyl)thieno[3,2-b]thiophene (71.73 mg, 0.15 mmol, 1 eq.), were dissolved in 3.0 mL of degassed anhydrous DMF inside of a dry microwave vial. To eventually remove water residuals, the reaction mixture was purged with argon for 20 minutes. Tris(dibenzylideneacetone)dipalladium(0) ($Pd_2(dba)_3$, 2.8 mg, 0.003 mmol, 0.02 eq.) and tris(o-tolyl)phosphine (P(*o*-tol)$_3$, 3.74 mg, 0.012 mmol, 0.08 eq.) were then added. The reaction mixture was purged with Ar for 5 additional minutes before being heated to 100 °C. During polymerization, the reaction mixture turned to a blue gel. The end-capping procedure was finally carried out after heating the reaction mixture for 9 hours. The end-capping procedure consists in the addition of 0.2 mL of degassed DMF, followed by the addition of $Pd_2(dba)_3$ and P(o-tol)$_3$ (1:8, $Pd_2(dba)_3$:P(o-tol)$_3$ molar ratio; Pd loading 0.0067 equiv.). Then, 2-(Tributylstannyl)thiophene (0.2 equiv) was added and the reaction was carried out at 120 °C for 15 minutes with continuous stirring. Finally, 2-bromothiophene (0.4 equiv) was added and the reaction was left to stir at 120 °C for other 15 minutes. After the end-capping procedure, the reaction mixture was left to cool down at room temperature. The reaction mixture containing the blue polymer was collected in a thimble. The mixture then underwent repeated Soxhlet extractions, carried out in methanol (16 h), acetone (16 h), hexane (16 h), THF (16 h) and chloroform (16 h) with the reaction mixture eluting in the chloroform fraction. The residual solvent was removed at a reduced pressure. After that, the polymer was reprecipitated in methanol from a chloroform solution. The polymer was finally collected by suction filtration and the dried at high vacuum conditions. The polymer was stored under argon atmosphere until used. The **pgBTTT** product is a solid of blue color (23 mg, 24% yield).

GPC (DMF, 45°C) M_n = 10 kDa, M_w = 24 kDa

The glycolated derivative of spiropyran (**OEG-SP**) was synthesized following the synthetic route depicted on Scheme S1.

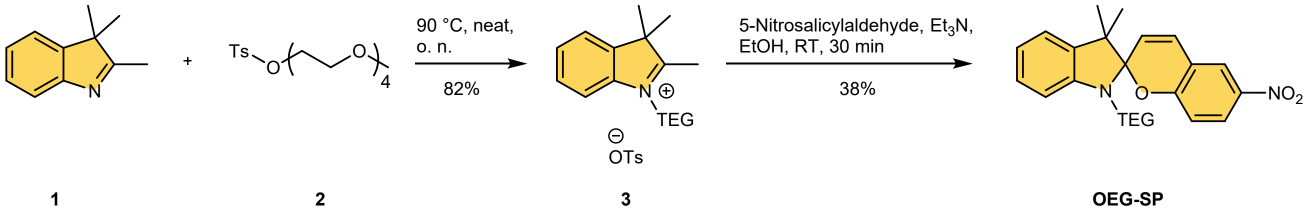

Scheme S1 – Synthetic scheme of **OEG-SP**.

2,3,3-trimethyl-1-(2,5,8,11-tetraoxatridecan-13-yl)-3H-indol-1-ium tosylate (**3**)

Indole **1** 1.50 g (9.42 mmol, 1.2 equiv.) was mixed with the toluate **2** 2.84 g (7.84 mmol, 1.0 equiv.) in a 20 mL vial and sealed with septum-equipped cap under N_2 atmosphere without any additional solvent. The neat reaction mixture was heated at 90 °C for 24 h with rapid stirring. Next, the mixture cooled to RT was mixed vigorously with Et_2O (10 mL) and left undisturbed for phase separation. After phases separated, the top Et_2O layer was decanted. The mixture was washed with Et_2O two more times, and dried in vacuum, yielding **3** as deep purple oil (3.38 g, 6.47 mmol, 82%). This hygroscopic oil was used directly in the next step without any further purifications.

3',3'-dimethyl-6-nitro-1'-(2,5,8,11-tetraoxatridecan-13-yl)spiro[chromene-2,2'-indoline] (**OEG-SP**)

To a mixture of indolium salt **3** 3.38 g (6.48 mmol, 1.0 equiv.) and 5-nitrosalicylaldehyde (1.08 g, 1.0 equiv.) in anhydrous EtOH (20 mL) Et_3N was added in one portion (0.90 mL, 0.66 g, 1.0 equiv.) upon stirring. The colour of the mixture immediately turned violet and stirring was continued for 1 h at RT. Next, the volatiles were removed in vacuum and the crude mixture was loaded on celite. The crude product was purified by flash column chromatography first (SiO_2, pentane:EtOAc = 1:4) and (SiO_2, DCM:MeOH, 8% of MeOH) yielding **OEG-SP** as slightly yellow oil (1.23 g, 2.47 mmol, 38%) solidifying upon standing. Upon storage, the solid changes to colour to red without affecting the purity of the compound.

The ^{1}H and ^{13}C nuclear magnetic resonance (NMR) and electrospray ionization (ESI) high-resolution mass spectrometry (HRMS) data are reported in Figures S1, S2 and S3, respectively.

^{1}H NMR ($CDCl_3$, RT, 500 MHz) δ 8.06 – 7.92 (m, 2H), 7.18 (td, J = 7.6, 1.3 Hz, 1H), 7.08 (dd, J = 7.3, 1.3 Hz, 1H), 6.93 – 6.82 (m, 2H), 6.74 (d, J = 8.8 Hz, 1H), 6.64 (d, J = 7.7 Hz, 1H), 5.91 (d, J = 10.3 Hz, 1H), 3.69 – 3.55 (m, 12H), 3.55 – 3.50 (m, 2H), 3.47 (dt, J = 14.1, 7.0 Hz, 1H), 3.37 (s, 3H), 3.32 (ddd, J = 14.8, 6.8, 5.1 Hz, 1H), 1.27 (s, 3H), 1.16 (s, 3H).

^{13}C NMR ($CDCl_3$, RT, 126 MHz) δ 159.7, 147.0, 141.1, 135.9, 128.2, 127.9, 126.0, 122.8, 122.4, 121.9, 119.7, 118.7, 115.6, 106.8, 106.8, 72.0, 70.8, 70.7, 70.7, 70.6, 69.4, 59.2, 52.9, 43.5, 26.0, 20.0. One OEG chain ^{13}C resonance was not observed.

ESI Pos HRMS $C_{27}H_{35}N_2O_7$ $[M+H]^+$: observed: 499.2429, calculated: 499.2439.

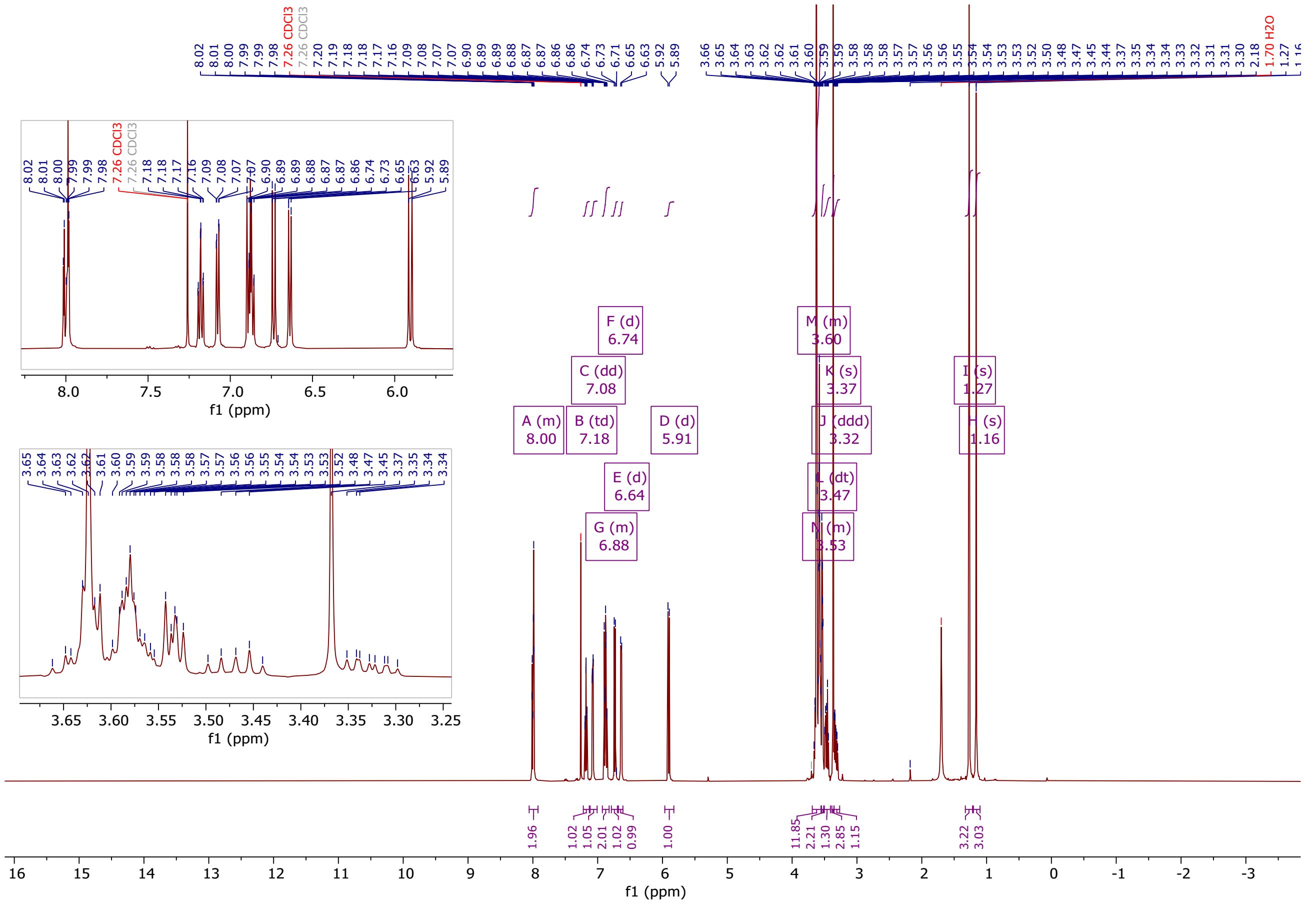

Figure S1 – ^{1}H NMR ($CDCl_3$, RT, 500 MHz) spectrum of **OEG-SP**

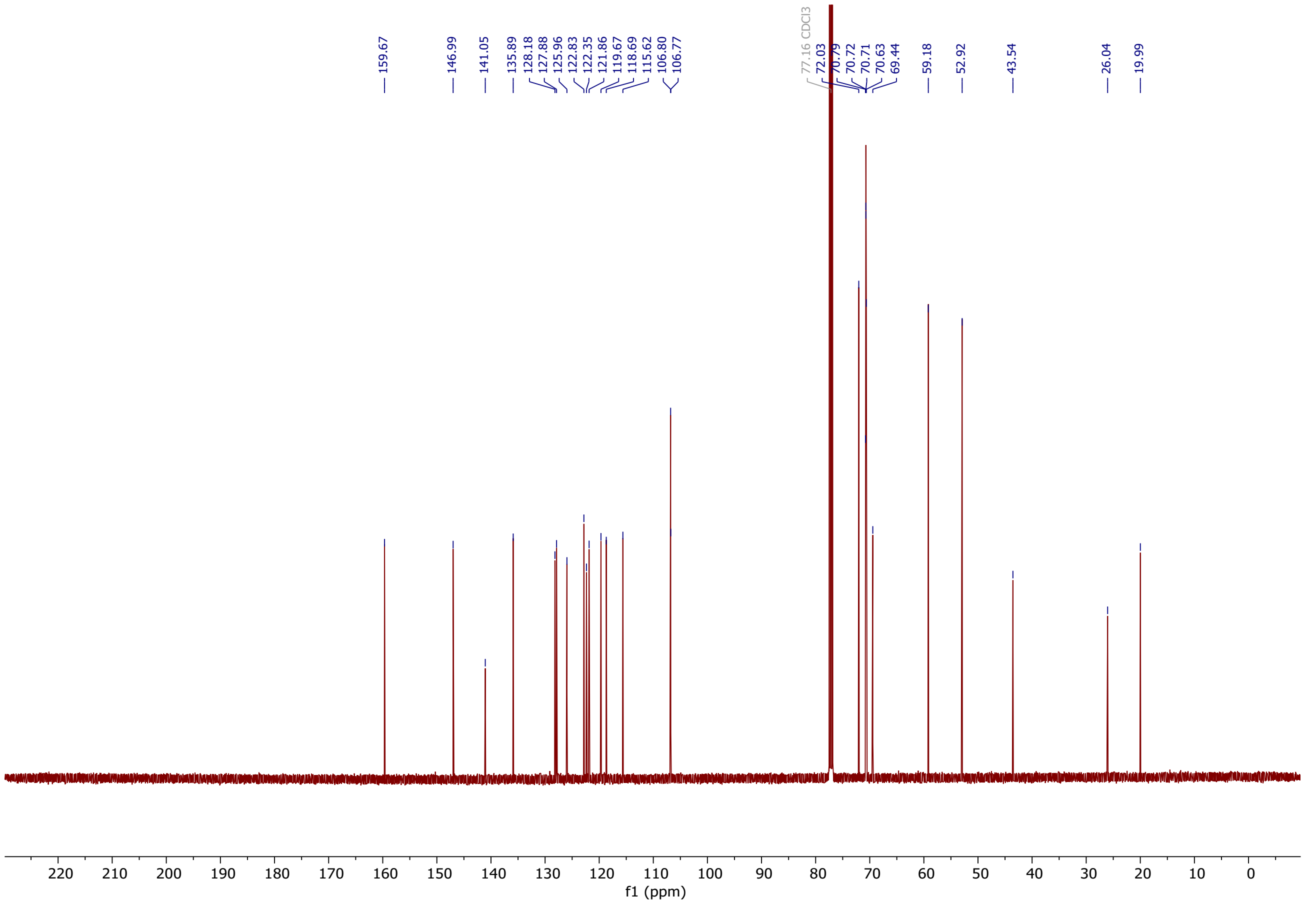

Figure S2 – ^{13}C NMR ($CDCl_3$, RT, 126 MHz) spectrum of **OEG-SP**

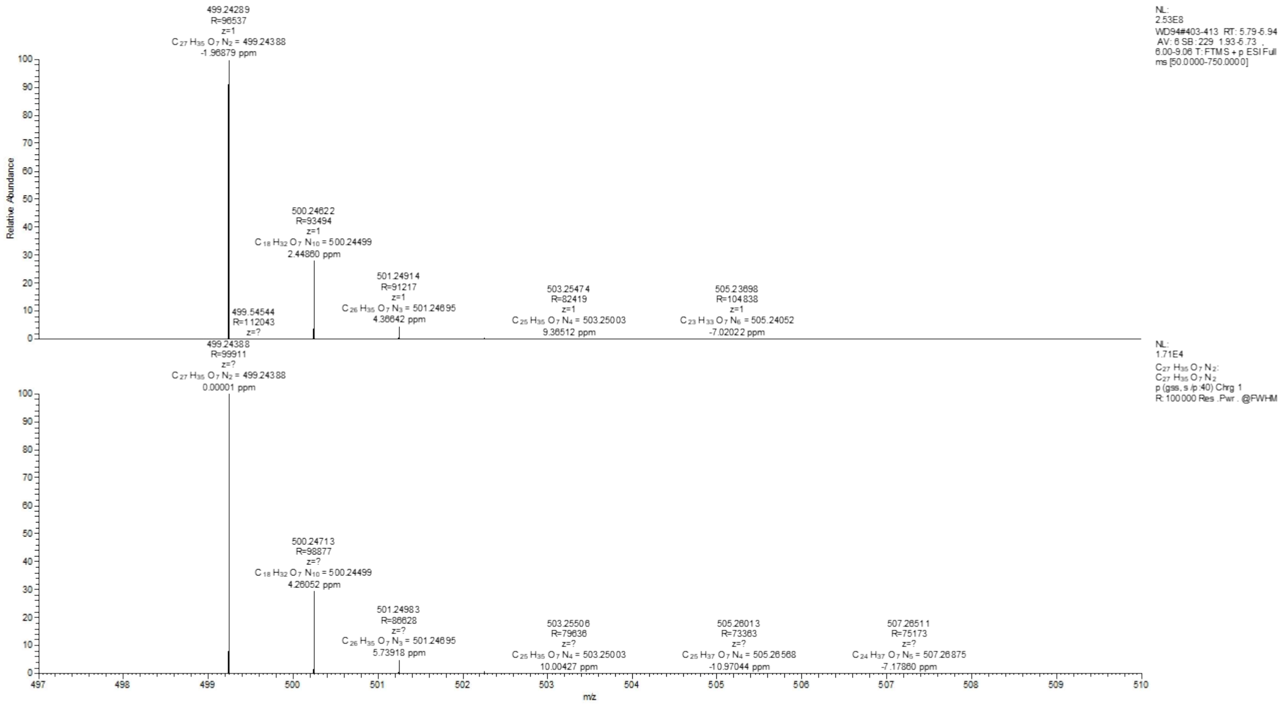

Figure S3 – HRMS spectrum of **OEG-SP**. Top: experimental. Bottom: calculated.

2 UV-Vis Photoswitching Experiments

The UV-Vis absorption spectra in solution were recoded in 1-cm quartz cuvettes loaded on a V-670 UV-Vis-NIR spectrometer (Jasco) equipped with a PAC-743R (Jasco) petlier cell changer. All the UV-Vis absorption spectra were recorded in HPLC-grade solvents without any further pretreatment. For solid-state UV-Vis spectroscopy, thin films were prepared by spin-coating diluted solutions of **OEG-SP** (DCM, 800 rpm), **pgBTTT** polymer ($CHCl_3$, 800 rpm) or **OEG-SP**/**pgBTTT** (1:4) blend ($CHCl_3$, 800 rpm) on ultraflat quartz substrates (Ossila) using a Spin150 spincoater (APT GmbH). These solutions were prepared by overnight stirring at 40 °C in sealed vials at concentrations ranging from 0.05 to 1 mg/mL. All the photoswitching experiments were performed in a dark room at ambient conditions.

The UV-Vis absorption spectra of thin films were recorded using a PAC-743R integrating sphere (Jasco) in transmission geometry. All spectra were baseline corrected using the Spectragryph software “simple baseline” algorithm. Irradiations were performed using LEDs (M365F1, M530F1, M365L2) purchased from Thorlabs Inc. These experiments were performed with two different LEDs controlled by a programmable driver to selectively switch on and off the LED light: (i) a ThorLabs M365F1/M365L2 UV-LED operating at 700 mA and emitting light at 365 nm with a power output of 3 W and (ii) a ThorLabs M530F1 operating at 1000 mA and emitting light at 530 nm with a power output of 5 mW.

UV-Vis Photoswitching Dynamics of OEG-SP in solution

The UV-Vis spectra of **OEG-SP** solubilized in methanol (MeOH) is reported in Figure S4a. Upon irradiation of the **OEG-SP** solution in MeOH with a 365-nm UV LED, an intense absorption band appears at around 570 nm. When the **OEG-SP** solution in $CHCl_3$ is irradiated by UV light, its color turns from a very pale yellow to a brilliant violet-blue. By irradiating the sample with a 530-nm LED, the system switches back to the SP form with consequent disappearance of the strong absorption band.

The same experiment can be performed for the **OEG-SP**/**pgBTTT** (1:4) blend system in MeOH solution (Figure S4b). Upon UV light irradition, the intense 570-nm band appears also in the UV-Vis spectra of the blend. This change is reversible as well by 530-nm light irradation.

The time decay of the MC form of **OEG-SP** was monitored in solution as a function of time in the dark at room temperature. The absorbance (A) of the characteristic peak of the MC form was recorded over time in a polar medium (MeOH) and a moderately polar solvent (THF). The decay curves are reported in Figures S4c and d. As observed in these figures, the photoisomerization process that converts the MC form to the SP form occurs much faster in THF than in MeOH. For a more quantitative evaluation of the decay process, the decay can be modelled by fitting A(t) with a series of exponential decay equations, each of which accounts for a chemico-physical occurring in the medium.

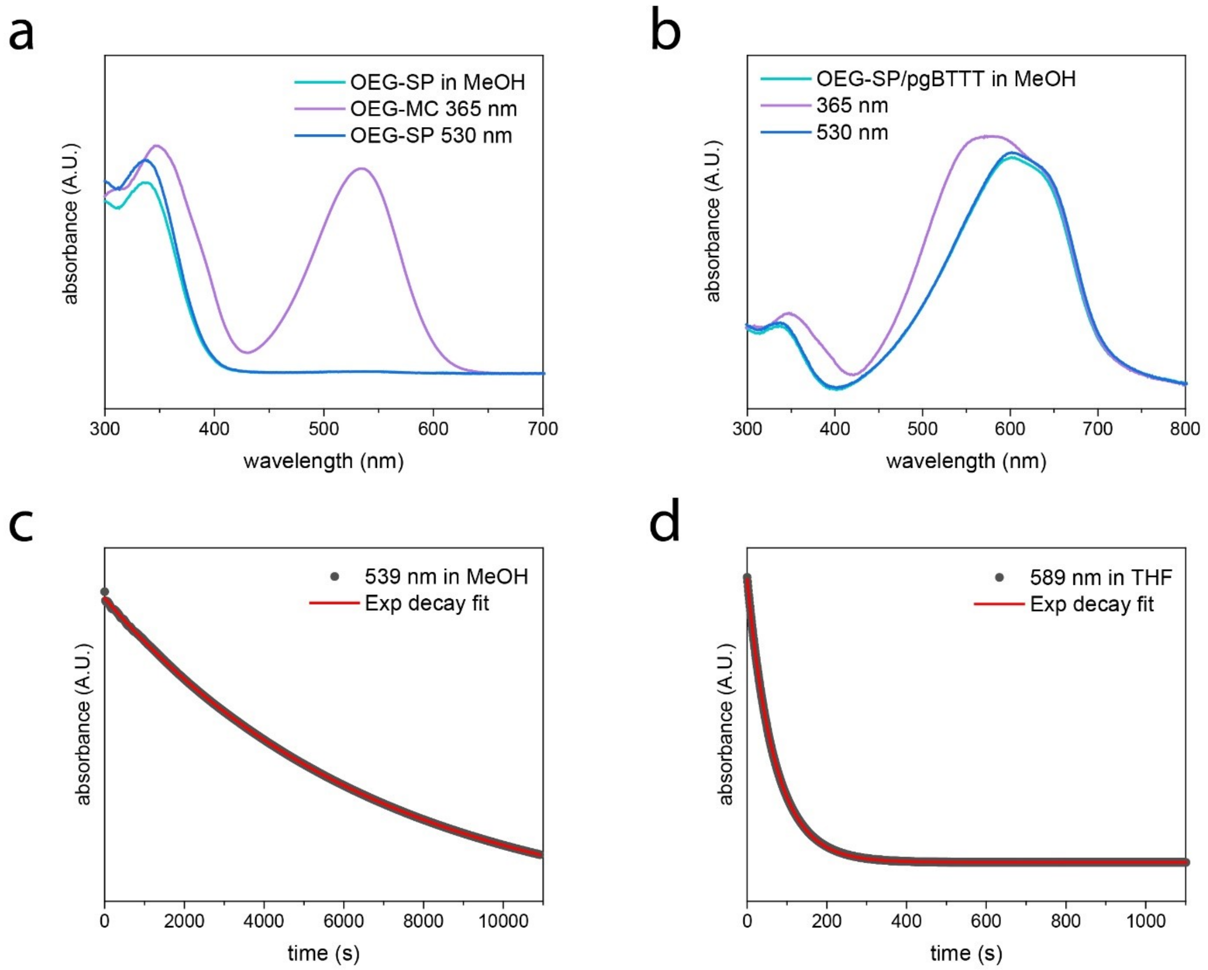

Figure S4 – UV-Vis characterization of the **OEG-SP** system. Reversible photoswitching of (a) **OEG-SP** and (b) **OEG-SP/pgBTTT blend** in a methanol solution. Decay of MC photoexcited state (c) in methanol (MeOH) solution and (d) in tetrahydrofuran (THF) solution. The solutions were first illuminated with the 365-nm UV LED (until no more color change could be seen) and, then, the decay of the absorbance associated with the main electronic transition was monitored via UV-Vis spectrophotometry. The data were fitted by an exponential decay equation (see Equation S1).

A(t) decay curves in solution can be fitted by a single exponential decay (Equation S1) to estimate the half-life ($t_{1/2}$) of the MC form (Equation S2) by extracting the time constant (τ) of the decay process.

$$A(t) = A_0 + A_1 \cdot e^{-\frac{t-t_0}{\tau}}$$

(Equation S1)

$$t_{1/2} = ln(2) \cdot \tau$$

(Equation S2)

A(t) is expressed by Equation S1 as the product of the starting absorbance (A_1) of the fully converted **OEG-MC** solution at the wavelength of the characteristic transition and a time-dependent exponential decay controlled by a time constant (τ). A_0 and t_0 are two fitting constants that assume negligible values but account for small corrections in residual absorbance and starting time of the decay. Equation S2 is then obtained from Equation S1 by finding the t value corresponding to $A(t_{1/2}) = A_1/2$.

The curve fitting is achieved with sufficient accuracy already with one exponential component in the fitting equation. This suggests that the photoisomerization process may occur via a single decay pathway. The half-lives of **OEG-MC** estimated by the fitting of decay curves are $t_{1/2\mathrm{MeOH}} \approx 80$ min and $t_{1/2\mathrm{THF}} \approx 45$ s.

UV-Vis Photoswitching Dynamics of OEG-SP at the solid state

The photoswitching in the solid state was performed on **OEG-SP** films that were drop-cast from $CHCl_3$ (Figure S5). The film of **OEG-SP** in the SP form was found being characterized by a pale yellow color that turns to a darker tint when deposited and equilibrated with ambient light. When the film was irradiated with a 365-nm UV LED, it turned to an intense dark purple colour. For drop-cast thin films deposited from $CHCl_3$ solutions, the SP form readily absorbs the environmental water contained in the ambient humidity. The surface appearance of the film turns from opaque to lucid upon swelling. The film in the MC form, instead, appears opaque as part of the absorbed water is returned to the ambient upon photoisomerization.

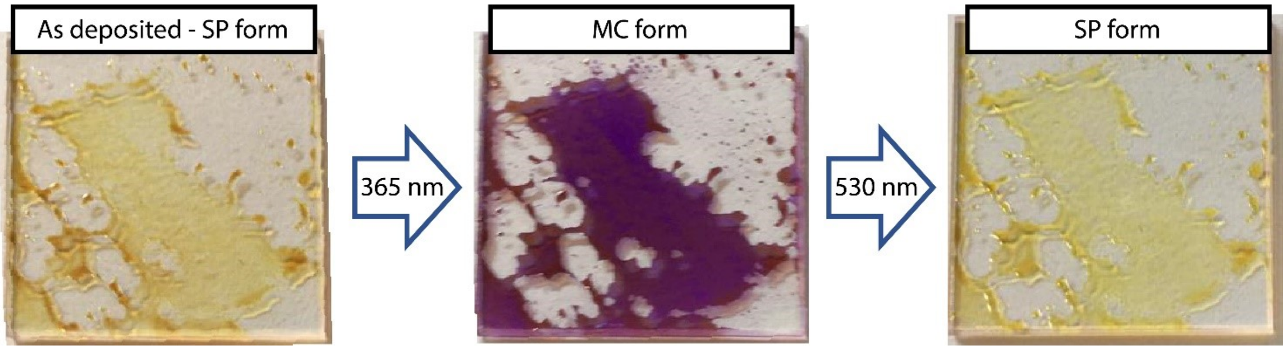

Figure S5 - Photographs of **OEG-SP** films drop casted from $CHCl_3$. The films are illuminated with either the 365-nm UV LED or the 530-nm visible LED to achieve reversible photoswitching.

The photostability of the thin film was monitored over five alternating UV (365 nm) and Vis (530 nm) irradiation cycles. **OEG-SP** shows negligible photo-fatigue over the course of the experiment, hence being reasonably stable at the solid state. However, a drastic change in the UV-Vis spectra of the photogenerated **OEG-MC**, indicative of the adsorption of water vapour (i.e., atmospheric moisture) by the film, was observed (Figure S6a). Over the course of the experiment, the lowest energy band characteristic of the **OEG-MC** form undergoes a gradual blue-shift (Figure S6b). This shift was quite substantial, reaching 20 nm between the first and the last UV cycle. Such change is typically indicative of the increased polarity of the medium and it originates from stabilization of the ground state accompanied by destabilization of the excited state.

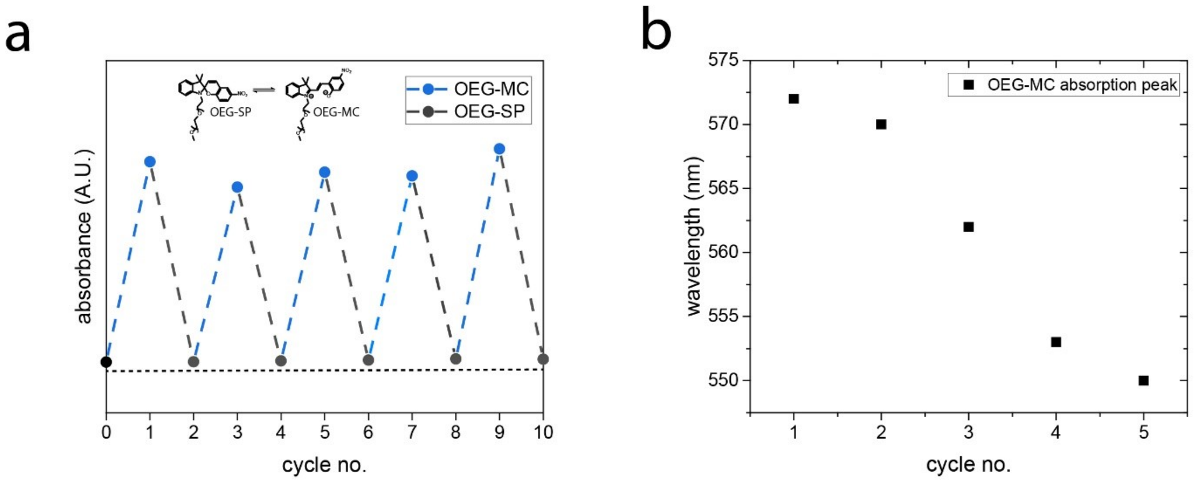

Figure S6 - UV-Vis spectral changes upon photoswitching of OEG-SP thin films. (a) Relative absorbance of the thin film at 570 nm as photoswitching cycles are performed at ambient conditions. (b) Progressive shift of the absorption peak maximum due to the absorption of environmental water.

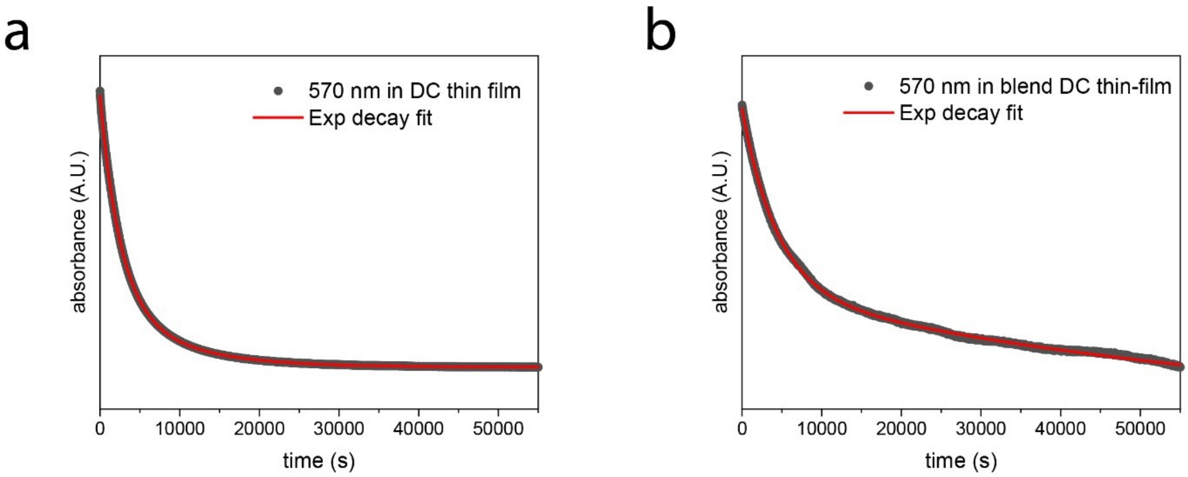

Figure S7 - Decay of MC form at the solid state. The drop-casted (DC) thin films deposited on quartz substrates were first illuminated with the 365-nm UV LED and the decay of the absorbance at 570 nm was monitored via UV-Vis spectrophotometry. (a) **OEG-SP** and (b) **OEG-SP/pgBTTT** blend. The data were fitted by a biexponential decay equation (see Equation S3). (a) τ_1 = 42 min, τ_2 = 145 min, (b) τ_1 = 73 min, τ_2 = 1146 min.

Investigating the photoswitching properties of **OEG-SP** at the solid state is important toward the understanding and optimization of the operation of devices when **OEG-SP** is blended with **pgBTTT**. The UV-Vis characterization of the **OEG-SP** system and its blend with **pgBTTT** is reported in the main text as Figure 1. The expression used for fitting the decay curve of **OEG-MC** at the solid state (Figure S6) is reported in Equation S3.

$$A(t) = A_0 + A_1 \cdot e^{-\frac{t-t_0}{\tau_1}} + A_2 \cdot e^{-\frac{t-t_0}{\tau_2}}$$ **(Equation S3)**

Compared to Equation S1, there is an additional exponential decay component, characterized by an amplitude A_2 and a time constant τ_2 that are distinctive of the additional process. This biexponential decay probably underlies two processes: one associated with the monomeric MC form (faster rate) and one associated with aggregated MC species (slower rate).

The rate of thermal recovery of OEG-SP from the MC-pgBTTT blend was measured from drop-casted thin films (Figure S7b). The kinetics of this process still follows the bi-exponential decay, however, with vastly different rates than the pure OEG-MC at the solid state (Figure S7a). The overall kinetics was found to be slower, which is consistent more polar environment of the blend and in line with the studies in the solution.

Leakage experiments during photoswitching of the blend thin film

During the photoswitching experiments performed on the OECT devices, the polydimethylsiloxane (PDMS) pool exhibited some degree of solid-state fluorescence emission indicating that the photochromic molecule somehow migrated to the polymer and possibly leaked into the electrolyte. PDMS is known for being hydrophobic, but a wide range of organic molecules can permeate its structure.[2]

As it can be observed from Figure S8, obtained after 10 minutes of irradiation with 365-nm light, the PDMS pool incorporates the photoswitch during the irradiation of the thin film in contact with the 0.5 M NaCl electrolyte. Since the electrolyte is in direct contact with both the thin film and the PDMS pool, a water mediated transport of OEG-MC from the polymer blend to PDMS can occur.
The UV-Vis spectrum of the electrolyte after 10 minutes of 365-nm of irradiation while in contact with the polymer blend shows that the photochromic additive leaked into the NaCl solution (black line, Figure S8a). For comparison, the spectrum obtained from mixing of 0.5 M NaCl in water with some OEG-SP powder and undergoing the same UV irradiation procedure is characterized by similar absorption peaks (red line, Figure S8a). The UV-Vis spectra have been collected with 0.5 M NaCl in water as a baseline. It can be observed that a significant amount of OEG-MC is solubilized in water, hence, OEG-MC is transferred from the thin film to the electrolyte and to the PDMS pool.

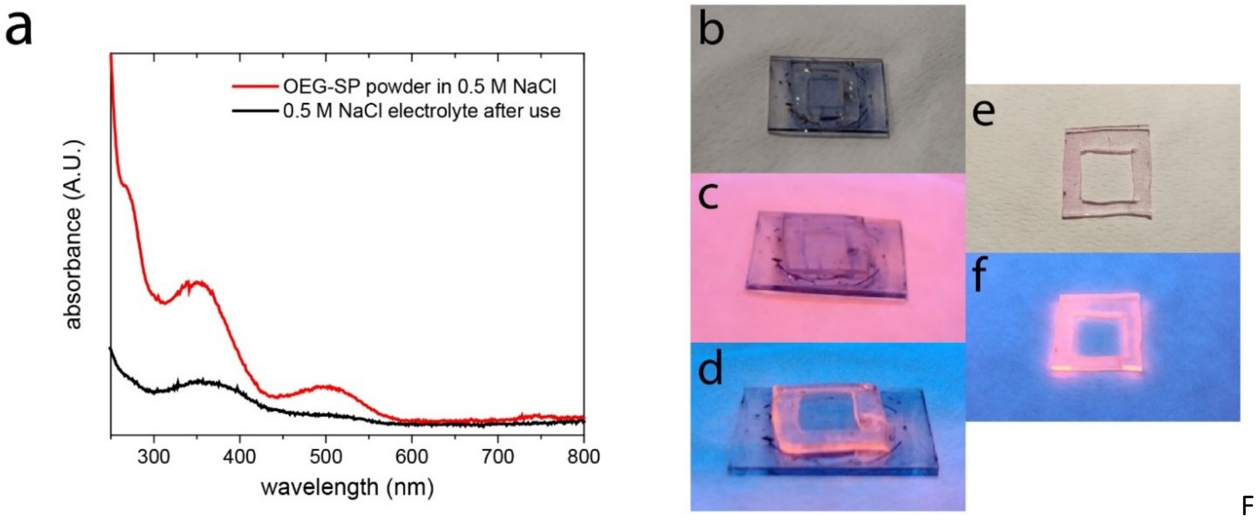

Figure S8 - Characterization of electrolyte solution and leakage of the photoswitching molecule into the PDMS pool. (a) UV-Vis absorption spectra OEG-SP solutions (0.5 M NaCl in water). The spectrum of the electrolyte collected after 10 minutes of UV irradiation while in contact with the blend (black) was compared with that obtained from a solution of the electrolyte and the **OEG-SP** powder that were mixed while irradiating with UV light for 10 minutes (red). (b) Photographs of the **OEG-SP/pgBTTT** blend deposited via drop casting on glass substrate and the PDMS pool containing the 0.5 NaCl electrolyte after 10 minutes of 365-nm light irradiation. Photograph in ambient light (b, e), with red light in dark room (c), with 365-nm light in dark room (d, f).

3 Electrical Characterization of OECTs

For the fabrication of OECT devices, quartz substrates were first prepatterned by thermal deposition of bottom source, drain and coplanar gate electrodes. The electrode layout was designed via CleWin layout editor and the substrate patterning was performed by laser lithography. Au electrodes consisting of a Cr underlayer (2 nm) and a Au layer (40 nm) were deposited at a rate of 0.1 Å/s and a base pressure of around 10^{-7} mbar (maximum pressure during deposition of 10^{-5} mbar) and obtained via a lift-off procedure. The device channels have width (W) = 300 µm and length (L) = 30 µm (W/L = 10, channel area of around 9×10^{-3} mm^2) and a coplanar gate electrode of rectangular shape (area around 3×4 mm^2) resulting in a gate to channel area ratio of around 10^3. Before the polymer deposition, the substrates were treated via UV-ozone (5 min) using a Novascan PDS Pro Series system to improve the polymer adhesion (except where differently indicated).

The active channel in OECT devices was fabricated via either drop casting (0.3 mg/mL in $CHCl_3$, resulting film thickness > 30 nm) or spin coating (10 s, 2500 rpm, 2000 rpm/s, 0.05 mg/mL in $CHCl_3$, resulting film thickness < 3 nm) of the polymer solution. For polymer blends, the same processing parameters were employed but spiropyran derivatives were added to the solution to give a 20% m/m **OEG-SP**/**pgBTTT** blend at a fixed **pgBTTT** concentration. The AFM height image of spin-coated samples is reported in Figure S9. As a last step of the fabrication the channel area was isolated by mechanical scratching of the deposited film to minimize current leakage. OECTs were operated in a 0.5 M NaCl in water electrolyte solution contained in a polydimethylsiloxane (PDMS) pool. For spin-coated devices, a top-gate geometry was used instead of the coplanar geometry. In this case, a Pt grid with dense weaving was used.

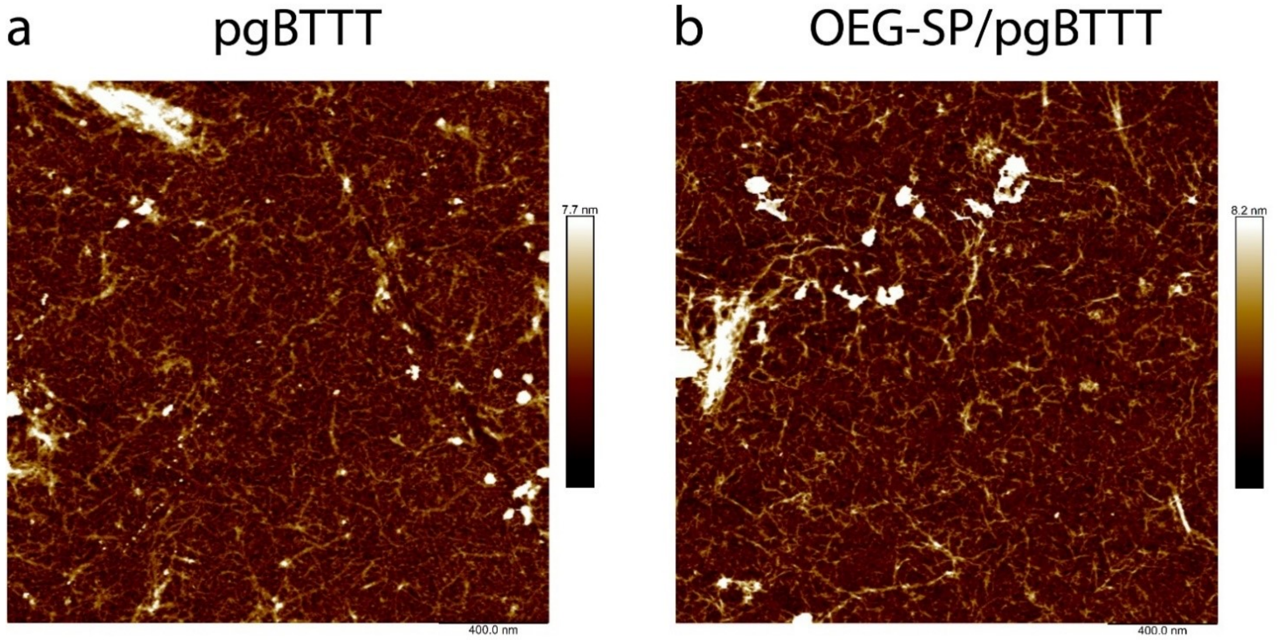

Figure S9 - AFM height images of spin-cast films of neat **pgBTTT** and **OEG-SP**/**pgBTTT** 20% m/m blends. Both films are deposited on a quartz substate from 0.05 mg/mL $CHCl_3$ solutions. Image size: 2×2 µm^2. (a) neat **pgBTTT**, Z-scale: 7.7 nm, thickness: 1.7 nm, R_{RMS}: 0.8 nm (b) **OEG-SP**/**pgBTTT**, Z-scale: 8.2 nm, thickness: 3.0 nm, R_{RMS}: 0.9 nm. R_{RMS} values are calculated over an area of 2×2 um^2.

The electrical measurements were carried out by using a Keithley 2636B SourceMeter unit to record electrical characteristics. With the parameters extracted from transfer curves, the mobility-volumetric capacitance product (μC*) can be estimated from the transconductance (Equation S4), if the device geometry and OECT operation parameters are known.[3]

$$g_m = \frac{Wd}{L} \mu C^* (V_G - V_{th})$$

(Equation S4)

For our OECT devices, W/L is 10 and d is 60 or 30 nm.

Stability and repeatability of transfer measurements based on OEG-SP/pgBTTT OECTs

To test the stability of the OECT electrical response at a given state (with either the photoswitching molecules in the **OEG-SP** or in the **OEG-MC** state) a repetition of three transfer curves with a delay of 10 s between each measurement was collected (Figure S10).

Multiple transfer curves can be collected from the same device with a dispersion of $I_{DS}(V_{GS})$ below 1% both after UV (**MC-pgBTTT**, Figure S10a) and visible light (**SP-pgBTTT**, Figure S10b) irradiation, with no increasing or decreasing drift observed within the timescale of the transfer curve measurements. The electrical behavior of the blend OECT is different from that of the neat **pgBTTT**, as in the latter device the contribution of the photoexcited carriers accounts for about 30% of the total current (for both UV and visible light) and τ_d is in the order of the minute (Figure 3d in the main text and Table S1). By irradiating the blend OECT with 365-nm light (with a process lasting 1-2 minutes to reach the steady state), the current decreases as shown in Figure 3a in the main text. By irradiating the blend OECT with 530-nm light (for about 5 minutes), a partial current recovery is achieved.

During photoswitching operations, OEG-MC is slowly solubilized in the electrolyte (Figure S8) and this removal of material from the active channel may alter the conductive pathways that existed in the original blend film. The film degradation process continues to occur until most of the photochromic molecules are solubilized, as evidenced by the I_{ON} stabilization in Figure 3b.

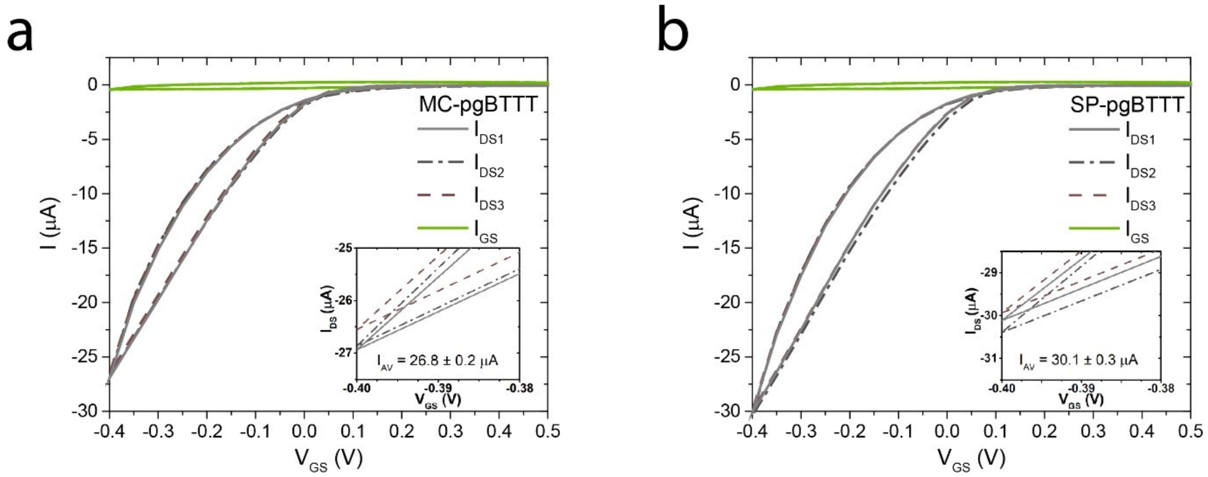

Figure S10 - Transfer curves collected from OECT devices at V_{DS}: -0.5 V, 0.5 M NaCl electrolyte, voltage sweep rate: 100 mV/s, W/L: 10. Repetition of 3 transfer curves collected from (a) SP-pgBTTT and (b) MC-pgBTTT. Magnification of $I_{DS}(V_{GS})$ in the maximum current region are shown in the inset graphs.

Effect of substrate treatment and channel depth

To test the effective influence of the substrate treatment in the modulation of the threshold voltage (V_{TH}), ultra-thin **pgBTTT** films have been spin casted on clean (5 min sonication in acetone and then isopropanol) and on UV/ozone-treated prepatterned quartz substrates from 0.05 mg/mL solutions of **pgBTTT** in $CHCl_3$. OECT devices fabricated on clean quartz are referred to as "**pgBTTT**/SiO_2". Those fabricated on UV-treated quartz are referred to as "**pgBTTT**/UV-SiO_2".

The resulting films have an average thickness of 1.5 nm (R_{RMS}: 0.8 nm) and 1.1 nm (R_{RMS}: 1.1 nm) for **pgBTTT**/UV-SiO_2 and **pgBTTT**/SiO_2, respectively (Figure S11). The use of UV/ozone prior to spin-coating deposition results in improved film-forming properties that are reflected on R_{RMS} values that are small compared to the thin-film thickness.

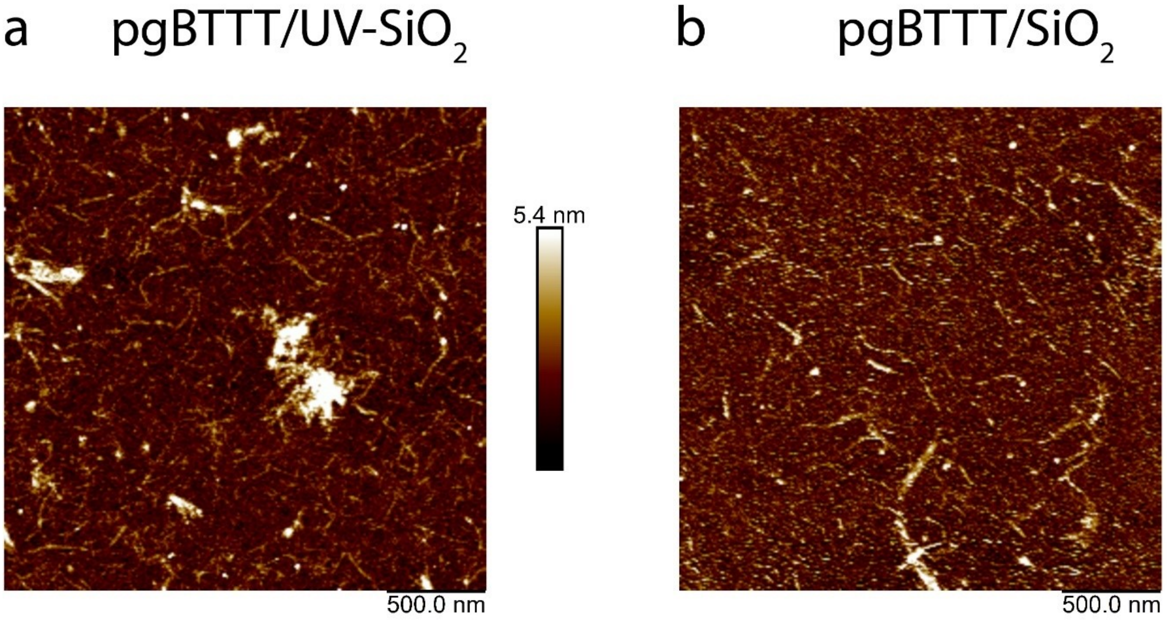

Figure S11- AFM height images of the spin-casted films of neat **pgBTTT** on different substrates. Both films are deposited on a quartz substate from 0.05 mg/mL $CHCl_3$ solutions. Image size: 2.5 × 2.5 µm². (a) **pgBTTT**/UV-SiO_2, Z-scale: 5.4 nm, thickness: 1.5 nm, R_{RMS}: 0.8 nm (b) **pgBTTT**/SiO_2, Z-scale: 10.5 nm, thickness: 1.1 nm, R_{RMS}: 1.0 nm. R_{RMS} values are calculated over an area of 2.5 × 2.5 um².

The transfer curves for OECT devices based on ultra-thin pgBTTT films are reported in Figure S12. The V_{TH} of these OECTs (around 300/400 mV), characterized by extremely small channel depths, is significatively shifted from that of thicker (60 nm) films on UV-SiO_2 substrates (−50 mV). This difference in V_{TH} indicates that thinner **pgBTTT** films (down to 2 nm thickness) possess different doping characteristics than those shown in the main text (Figure 3c). V_{TH} can be controlled by substrate effects or ion diffusion originating from the electrolyte solution. Both effects are more susceptible to change in thinner films thus providing a way to control V_{TH} via either a substrate treatment or by tuning the channel depth. Here, V_{TH} was found to change from +400 mV (2-nm-thick films) to −50 mV (60-nm-thick films) with a previous report of −220 mV for films thicker than 100 nm.[1] Another example was reported by Cicoira et al. who found that the V_{TH} of PEDOT:PSS OECTs (depletion mode devices) was increasing with thickness, meaning that a more intense gate voltage was needed to dope the material (and thus deplete the charge carriers in the channel) at a larger channel thickness.[4]

The data in Figure S12 also indicates that the UV/ozone pretreatment of the SiO_2 substrate can lead to a further shift of V_{TH} towards more positive values (V_{TH} stands at about +300 mV and +400 mV for SiO_2 and UV-SiO_2 substrates, respectively). The UV/ozone treatment can influence the doping state of the polymer by providing free silanol sites and fixed charges that may interact with the OSC material and consequently shift the V_{TH}.[5] The interplay between substrate wettability and channel depth is thus key to the tuning of the V_{TH} in OECTs.

For a fair comparison of the performance of the OECTs, g_m values at the same voltage overdrive (V_{OV} = 0.45 V), 3.4 µS and 6.4 µS for SiO_2 and UV-SiO_2 substrates, respectively, normalized by the channel depth (d) should be considered. Under these premises, the ratio between the µ values is about a factor 1.4 in favor of the UV-SiO_2 OECTs, suggesting that the difference in the electrical characteristics is not as pronounced as it seemed from a simple comparison of the maximum I_{ON}.

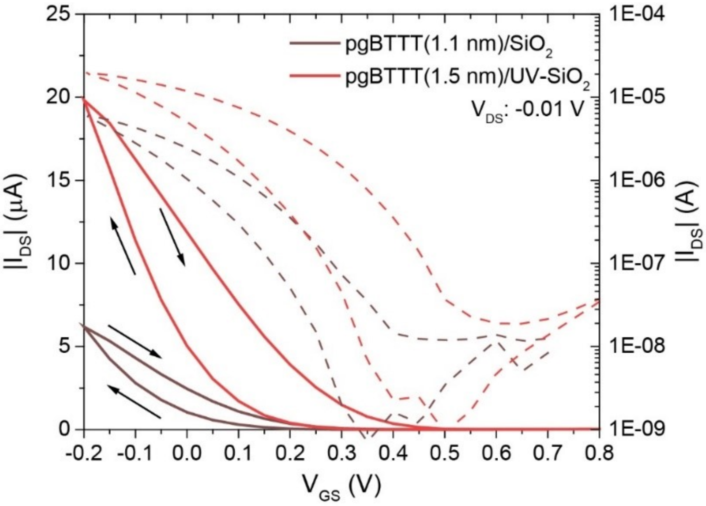

Figure S12 - Transfer curves of **pgBTTT** OECT devices recorded at low bias (V_{DS}: -0.01 V) in 0.5 M NaCl at ambient conditions. The OECT devices were fabricated on clean quartz (SiO_2, brown) and UV-treated (UV-SiO_2, red) substrates via spin coating of 0.05 mg/mL **pgBTTT** solutions in $CHCl_3$. Voltage sweep rate: 100 mV/s. Linear (solid) and logarithmic (dashed) scales, the applied V_{DS} and the arrows illustrating the voltage sweep direction are reported in the figure.

Electrical Characteristics of neat pgBTTT OECTs

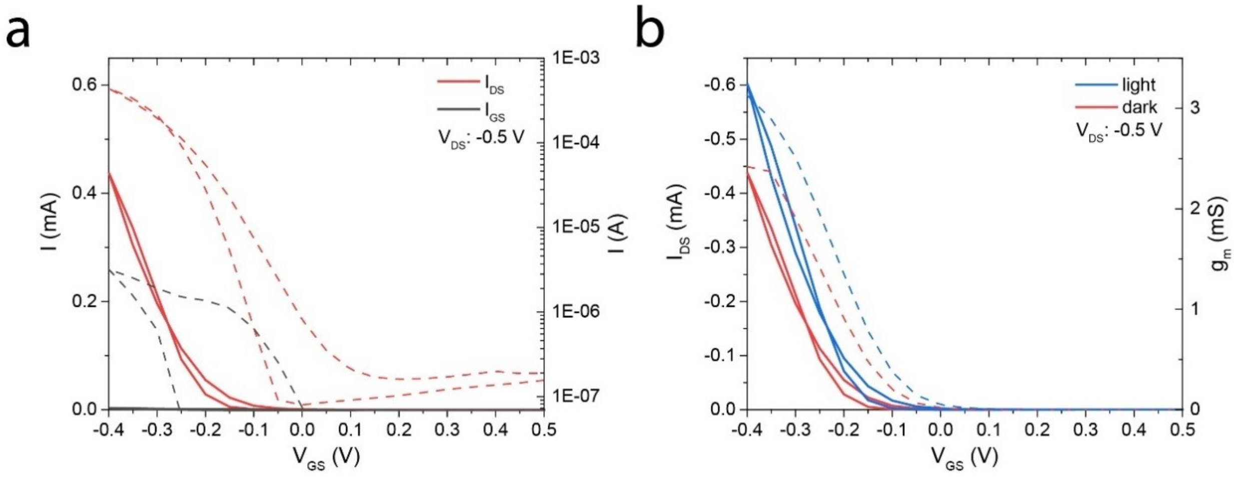

Figure S13 - Transfer characteristics of **pgBTTT** OECTs and photocurrent response. (a) Transfer and leakage curves of **pgBTTT** OECT devices recorded in 0.5M NaCl (saturation regime, dark conditions). Solid and dashed curves are reported in linear and logarithmic scale, respectively. (b) Transfer characteristics of **pgBTTT** OECT devices in dark and under constant illumination with 530 nm light from a green LED. The transconductance (g_m) is also reported with a dashed line. All transfer curves were recorded at V_{DS}: -0.5 V. 0.5 M NaCl electrolyte. Voltage sweep rate: 100 mV/s. W/L: 10.

Transient photocurrent in neat pgBTTT OECTs

To evaluate the timescale of the process of photoexcitation of charge carriers, the growth and decay of the photocurrent were monitored as a function of the illumination time, i.e., a chronoamperometry $I_{DS}(t)$ at the device operation conditions (V_{GS}: −0.4 V and V_{DS}: −0.5 V) was performed during alternate irradiation with the 530-nm LED (Figure S14). Note here that chronoamperometric measurements on gated OECT devices do not provide a constant current immediately at the start of the measurement.[6] A transient current is associated with the switching of the OECT to the ON state, hence the photocurrent experiments were delayed by about 1-2 minutes after the bias application to achieve a steady state condition.

From the $I_{DS}(t)$ response of OECT under different light conditions one can estimate the photocurrent growth (τ_g) and decay (τ_d) time constants. The $I_{DS}(t)$ response can be fit by a non-linear growth/decay equation (Equation S5) to estimate τ values during the growth and the decay of the transient photocurrent curve. Equation S5 is expressed as a current (I_0) and time (t_0) offsets, a pre-exponential factor (A) that differentiate between for growth (−) and decay (+) behavior, and the time constant (τ).

$$I(t) = I_0 + A \cdot e^{-\frac{t - t_0}{\tau}}$$ **(Equation S5)**

The photocurrent τ values for **pgBTTT** OECTs are $\tau_g = 9 \pm 1$ s and $\tau_d = 16 \pm 2$ s, meaning that it takes a maximum time period of around one minute (> 3τ) for the **pgBTTT** system to stabilize once a steady light condition is set during device operation.

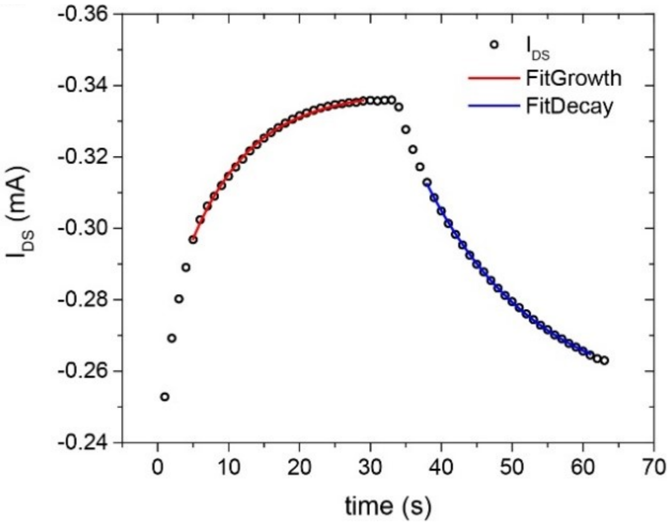

Figure S14 - Photocurrent response of neat **pgBTTT** OECTs collected at $V_{GS} = -0.4$ V and $V_{DS} = -0.5$ V. (a) OECT current response during and after continuous illumination with a 530-nm LED. The curves obtained by fitting of the I(t) data during the growth (red) and the decay (blue) of the current are reported in the same graph.

The time constants associated with the decay of photocarriers when the OECT is periodically switched on and off might differ from the ones obtained for continuous device operation. It is thus very important to verify if photogenerated carriers have different relaxation dynamics when the device is in the OFF state for some time during device switching. The stabilization of the transfer characteristics as a function of time has been thus investigated by photostimulated the **pgBTTT** OECT system for 2 minutes with either the 365-nm or the 530-nm LED to reach a steady state. Then, after switching off the light source, the transfer curves were consecutively collected every 20 s to determine the time dependence of the maximum I_{ON} and of the V_{TH} values. Since every transfer curve starts at positive V_{GS} values (in the OFF state) and the maximum I_{ON} value is obtained at t = 10 s, these measurements have a time resolution of 20 s and an initial time offset of 10 s. The decay curves of I_{ON} and V_{TH} are shown in Figure 3d in the main text. The data have been fitted with Equation S5 (adapted for V_{TH}) and the resulting τ_d fitting parameters are shown in Table S1.

Table S1 - Decay time constants (τ_d) for I_{ON} and V_{TH} OECT parameters obtained by non-linear fitting of the transfer curves collected at $V_{GS} = -0.4$ V and $V_{DS} = -0.5$ V from neat **pgBTTT** devices.

Sample	I_{ON} 365 nm	I_{ON} 530 nm	V_{TH} 365 nm	V_{TH} 530 nm
τ_d (s)	60 ± 10	45 ± 6	27 ± 2	27 ± 4

For an intermittent operation of the **pgBTTT** OECT devices, it is found that the decay time of the photocurrent is around one minute at worst. Whatever change in the device ON current provoked by the OECT irradiation with UV or visible light at the wavelength of the tested LEDs decrease by at least 63% of the original value during the first minute.

Stability and repeatability of transfer measurements based on neat pgBTTT OECTs

To test the stability of the basic OECT electrical response of neat **pgBTTT** devices a repetition of three transfer curves with a delay of 10 s between each measurement was collected (Figure S15).

Multiple transfer curves can be collected from neat **pgBTTT** devices (Figure S15). A steady state is reached prior to the application of the gate voltage sweep. We can exclude any effect deriving from device instabilities, as neat **pgBTTT** OECTs characterized in the dark show a device-to-device variability below 2% with no increasing or decreasing drift.

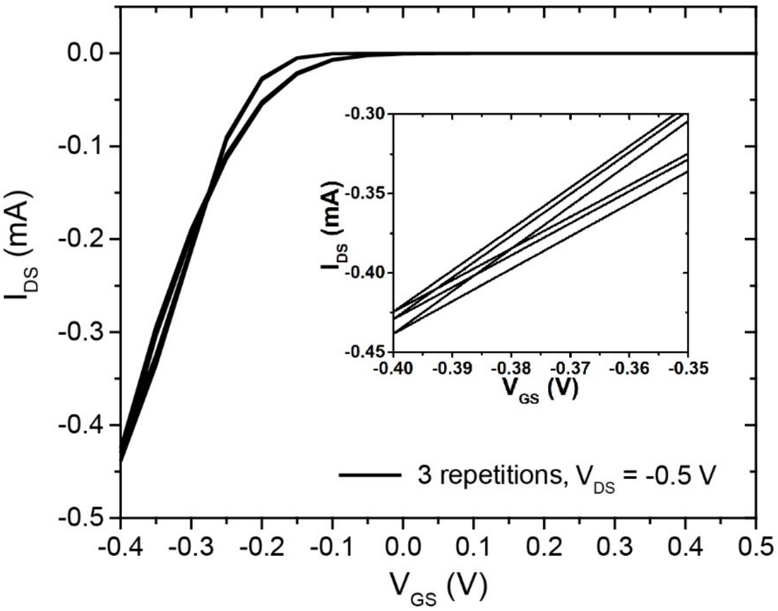

Figure S15 - Transfer curves collected on neat **pgBTTT** OECTs collected at $V_{DS} = -0.5$ V, 0.5 M NaCl electrolyte, voltage sweep rate: 100 mV/s, W/L: 10. Inset: Magnification of $I_{DS}(V_{GS})$ at V_{GS} in the maximum current region.

4 Electronic Characterization

Macroscopic Kelvin Probe (KP) and photoemission yield spectroscopy in air (PYSA) were performed on **pgBTTT**, **OEG-SP** and **OEG-SP/pgBTTT** thin films obtained via drop casting from $CHCl_3$ on conductive ITO-coated quartz substrates. ITO substrates were first sonicated in acetone (5 min) and isopropanol (5 min) and then treated via UV/ozone (5 min, Novascan PDS Pro Series). A drop casting of $CHCl_3$ solvent was done blank ITO substrates prior to KP and PYSA measurements. The electrochemical doping of polymer films resembling the channel material was done by applying a bias voltage of $V_{GS} = -0.5$ V for 60 s on a Pt-Ir wire electrode immersed in a 0.5 M NaCl solution (water electrolyte) kept in contact with the active material. The dedoping was similarly done, by applying $V_{GS} = +0.5$ V instead. The samples were dried by a stream of dry N_2 before analysis. PYSA measurements were performed at light spot intensity of 500 nW. Note that during the PYSA experiments the spiropyran sample underwent no significant color change upon UV irradiation (about 5 minutes) as the effective power of the UV beam is too low to induce the photoisomerization within the time of the measurement. Instead, after illumination with a UV LED at 365 nm (3 W) for the same period of time it completely turned to a dark violet color.

Effect of UV irradiation

To evaluate the effect of UV irradiation on the two material components, further KP and PYSA experiments were performed upon UV illumination for few minutes (Table S2).

Table S2 - IE and E_F of drop-casted pgBTTT and OEG-SP films on Au before and after irradiation with a 365-nm UV LED.

Sample		**pgBTTT**	**OEG-SP**
Before UV	**IE (eV)**	5.33 ± 0.06	5.68 ± 0.01
	E_F (eV)	4.46 ± 0.02	4.58 ± 0.02
After UV	**IE (eV)**	5.33 ± 0.05	5.65 ± 0.03
	E_F (eV)	4.51 ± 0.01	4.41 ± 0.02

5 References:

1 R. K. Hallani, B. D. Paulsen, A. J. Petty, R. Sheelamanthula, M. Moser, K. J. Thorley, W. Sohn, R. B. Rashid, A. Savva, S. Moro, J. P. Parker, O. Drury, M. Alsufyani, M. Neophytou, J. Kosco, S. Inal, G. Costantini, J. Rivnay and I. McCulloch, J. Am. Chem. Soc., 2021, **143**, 11007–11018.

2 J. M. Watson and M. G. Baron, J. Membr. Sci., 1996, **110**, 47–57.

3 S. Inal, G. G. Malliaras and J. Rivnay, Nat. Commun., 2017, **8**, 1767.

4 P. Kumar, Z. Yi, S. Zhang, A. Sekar, F. Soavi and F. Cicoira, Appl. Phys. Lett., 2015, **107**, 053303.

5 A. Wang, I. Kymissis, V. Bulović and A. I. Akinwande, Appl. Phys. Lett., 2006, **89**, 112109.

6 P. R. Paudel, M. Skowrons, D. Dahal, R. K. Radha Krishnan and B. Lüssem, Adv. Theory Simul., 2022, **5**, 2100563.